Res Chem Intermed
https://doi.org/10.1007/s11164-018-3490-1

Synthesis and biological evaluation of novel triazole-biscoumarin conjugates as potential antitubercular and anti-oxidant agents

Ashruba B. Danne[1] · Amit S. Choudhari[2] · Dhiman Sarkar[2] · Jaiprakash N. Sangshetti[3] · Vijay M. Khedkar[4] · Bapurao B. Shingate[1]

Received: 8 March 2018 / Accepted: 22 May 2018

Abstract The synthesis of a new series of triazole-biscoumarin conjugates by using a molecular hybridization approach is described. The newly synthesized compounds **6a–k** were evaluated for their in vitro antitubercular activity against active and dormant *Mtb* H37Ra and anti-oxidant activity against DPPH radical scavenging. Molecular docking simulations for the antitubercular activity showed that the conjugates **6a–k** bind in the pocket of the DprE1 enzyme. Most of the conjugates displayed good antitubercular activity against both the active and dormant *Mtb* H37Ra strain. The compound **6h** displayed very good antitubercular activity against dormant *Mtb* H37Ra with an IC_{50} value of 1.44 μg/mL. Most of the synthesized conjugates exhibit excellent anti-oxidant activity with an IC_{50} of less than the standard BHT. Compound **6b** is the most active among all the conjugates with an IC_{50} value of 08.17 ± 0.11 μg/mL. The molecular docking study shows good agreement between the observed antitubercular activity and the binding affinity.

Electronic supplementary material The online version of this article (https://doi.org/10.1007/s11164-018-3490-1) contains supplementary material, which is available to authorized users.

✉ Bapurao B. Shingate
bapushingate@gmail.com

[1] Department of Chemistry, Dr. Babasaheb Ambedkar Marathwada University, Aurangabad 431004, India

[2] Combi-Chem Bio-Resource Center, Organic Chemistry Division, CSIR-National Chemical Laboratory, Pune 411008, India

[3] Y. B. Chavan College of Pharmacy, Dr. Rafiq Zakaria Campus, Aurangabad 431001, India

[4] Department of Pharmaceutical Chemistry, Shri Vile Parle Kelavani Mandal's Institute of Pharmacy, Dhule, Maharashtra 424001, India

Published online: 31 May 2018

Graphical Abstract

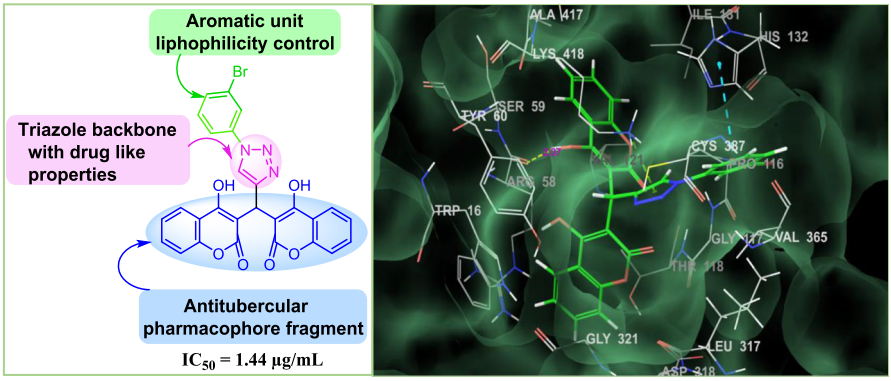

Keywords Antitubercular activity · Anti-oxidant activity · 1,2,3-Triazoles · Biscoumarins · Molecular docking

Introduction

The coumarin moiety has been used as a pharmacophore unit for the last two centuries. Many drugs bearing the coumarin moiety are used as anticoagulants, antibiotics, insecticides and pesticides. Synthetic organic chemists and biologists have paid attention to the synthesis of coumarin derivatives, because they exhibit various biological activities such as anticancer [1], anti-breast cancer [2], anti-Alzheimers [3], anti-oxidant [4], anti-influenza [5], antidepressant [6], antihepatitis C [7], anti-inflammatory [8] and antitubercular [9]. Synthetic and naturally occurring biscoumarin scaffolds have attracted considerable attention in medicinal chemistry. The biscoumarin derivatives are of biological importance because of their ability to form hydrogen bonding via two hydroxyl groups and show various biological activities including α-glucosidase [10], anticoagulant [11], antimicrobial [12], (HIV-1 IN) inhibitor [13], urease inhibitors [14], enzyme inhibitory activity [15], antibacterial, antitumor [16], anti-oxidant [17] and c-Met inhibitors [18]. Synthesis of coumarin fused or linked with different heterocyclic derivatives has been gaining importance over the last few decades in medical and chemical research [19].

The term, "Click Chemistry" was introduced for the first time by the Sharpless research group [20]. It is a 1,3-dipolar cycloaddition reaction between alkyne and azide catalyzed by Cu(I), selectively giving 1, 4-disubstituted-1,2,3-triazoles [21–24]. The 1,2,3-triazole pharmacophore unit containing the drugs 5-amino-1-(3,5-dichloro-4-(4-chlorobenzoyl)benzyl)-1H-1,2,3-triazole-4-carboxamide (CAI), Cefatrizine and Tazobactam are available in the market (Fig. 1). The 1,2,3-triazole is a bioisostere of the amide [25–28]. The 1,2,3-triazole nucleus has broad pharmaceutical and medicinal applications including α-

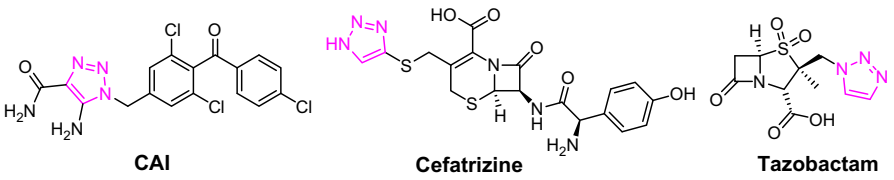

Fig. 1 Structures of 1,2,3-triazole-containing drugs

glycosidases [29], antimicrobial [30], antifungal [31], antiviral [32] and antitubercular activity [33–38].

There are several reports on the synthesis of 1,2,3-triazole-coumarin conjugates and their biological evaluation, such as antifungal, anti-oxidant [39], antitumor [40], antimicrobial [41–43], 5-lipoxygenase inhibitor [44], anti-inflammatory [45] and antimalarial [46] activities. The molecules (**A**–**D**) [47–50] bearing coumarin and 1,2,3-triazole as pharmacophoric groups, the complex of biscoumarin (**E**) [51] and other related compounds [52] display better antitubercular activity (Fig. 2).

Tuberculosis (TB) is a chronic contagious airborne disease caused by the mycobacterial pathogen *Mtb* [53]. According to WHO, 1.5 million peoples died and 9 million new TB cases were reported in 2013 [53]. The Bacilli Calmette–Guerin vaccine is used as chemotherapy for the treatment of TB [54], and the drugs Bedaquiline and Delamanid are also used for the treatment of multidrug-resistant (MDR) TB. However, the surge of MDR-TB and extensively drug-resistant TB does not respond to the first-line drugs and also the totally drug-resistant TB has been reported [55, 56]. This brings challenges for the researcher to design hybrid

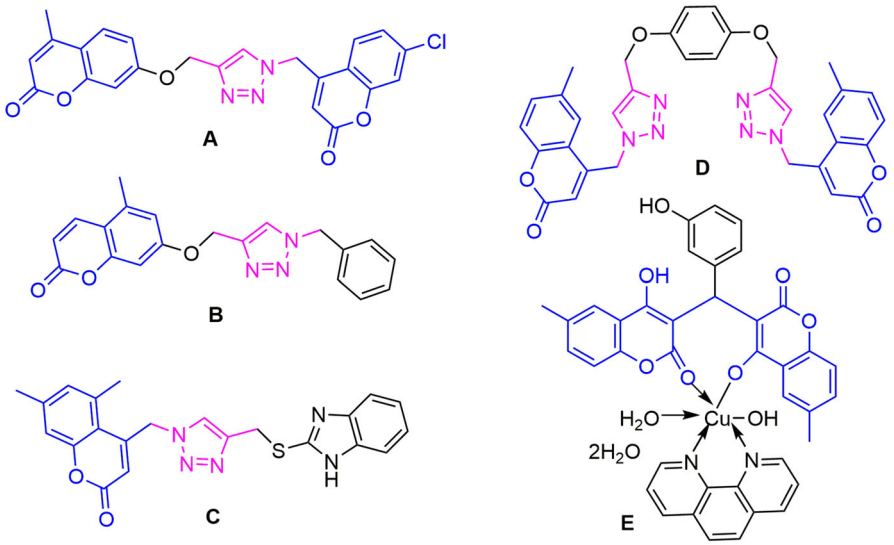

Fig. 2 1,2,3-Triazole-coumarin conjugates (**A**–**D**) and biscoumarin (**E**) shows good antitubercular activity

molecules by molecular hybridization of different bioactive substances as a newer, potent and more effective prototype antitubercular agent having a novel mode of action.

Free radicles are generated during aerobic respiration. The ROS acting as free radicles play a vital role in the human body, but may also exert toxic effects [57]. Our body develops a defence system to minimize the damage done by ROS by producing free radical scavengers including peroxidase, dismutase, catalase enzymes, cytochrome and glutathione [57]. There are several natural hydrophilic anti-oxidants such as sinapic, *p*-coumaric, caffeic and ferulic acids which are present in vegetables, fruits, herbs and spices [58]. Due to this, there is a need to develop better new anti-oxidant agents.

In view of the above and in continuation [39, 48, 59–66] of our program towards the development of new bioactive molecular hybrids, and the reported lead conjugates (**A**, **D** and **E**) having coumarin and triazole as a pharmacophoric groups, and the advanced molecular hybridization approach (Fig. 3), here, we would like to report the synthesis of novel 1,2,3-triazole-incorporated biscoumarin conjugates and the evaluation of their antitubercular and anti-oxidant activity. A molecular docking study of the synthesized conjugates were also performed.

Experimental

Materials and methods

Reagents were purchased from Spectrochem, Sigma Aldrich, and Alfa Aesar and used without further purification. Analytical thin-layer chromatography (TLC) was monitored with Merck Silica Gel 60 F_{254} and the spots were visualized using

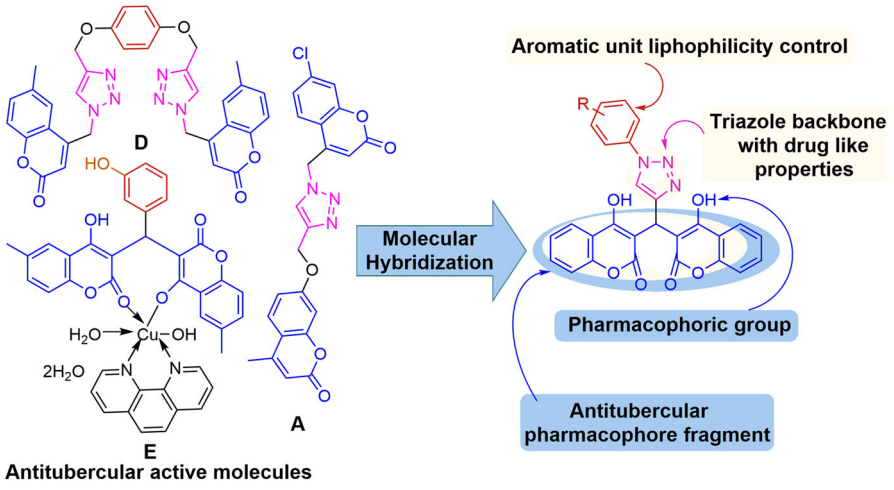

Fig. 3 Molecular design strategy for 1,2,3-triazole-coumarin conjugates

ultraviolet (UV) light with an excitation wavelength of 254 nm. Melting points were obtained on an open capillary electrothermal apparatus and are uncorrected. Infrared (IR) spectra were measured on an Alpha Brucker FT-IR spectrophotometer. The identity of the compounds were confirmed by NMR. ^{1}H and ^{13}C NMR spectra were obtained on Bruker Advance 400 and 100 MHz spectrophotometers, respectively. The compounds were solubilized in $CDCl_3$ and DMSO-*d6* with TMS used as an internal standard. The chemical shifts (δ) are expressed in parts per million (ppm). Multiplicity of the signals is shown as singlet (*s*), doublet (*d*), triplet (*t*), quartet (*q*), multiplet (*m*), and doublet of doublets (dd), and coupling constants *J* are given in Hz. High-resolution mass spectrometry (HRMS) experiments were performed for the exact mass determination of synthesized compounds.

General procedure for preparation of 6a–k

In a round-bottom flask equipped with a magnetic stirring bar, a mixture of triazole aldehyde **4a**–**k** (1.0 mmol) and 4-hydroxycoumarin **5** (2.0 mmol) in ethanol-acetic acid was refluxed for 4–6 h. The progress of the reaction was monitored by TLC. After completion of the reaction, the resulting mixture was concentrated under reduced pressure followed by the addition of 30 mL ice water. The obtained solid was filtered, dried and recrystallized from ethanol–acetic acid to obtain the pure products **6a**–**k** in good yields.

Spectral data of compounds

3,3′-((1-Phenyl-1*H*-1,2,3-triazol-4-yl)methylene)bis(4-hydroxy-2*H*-chromen-2-one) (**6a**) The compound **6a** was prepared according to general procedure using aldehyde **4a** and 4-hydroxycoumarin **5**, in 86% yield. Mp 246–248 °C. IR *v* max/cm^{-1} 3363, 1655, 1606, 1539, 756. ^{1}H NMR (400 MHz, DMSO-d_6) δ 8.17 (*s*, 1H), 7.85 (*t*, *J* = 12.0 Hz, 4H), 7.53–7.47 (m, 4H), 7.40 (*t*, *J* = 7.3 Hz, 1H), 7.23 (*d*, *J* = 8.3 Hz, 4H), 6.38 (*s*, 1H). ^{13}C NMR (100 MHz, $CDCl_3$ + DMSO-d_6) δ 167.9, 164.5, 152.5, 149.5, 136.8, 130.8, 129.5, 127.9, 124.2, 122.7, 120.1, 120.0, 119.6, 115.3, 102.8, 29.4. HRMS (ESI-TOF, $[M + H]^+$): *m*/*z* calcd for $C_{27}H_{17}N_3O_6$, 480.1195; found, 480.1193.

3,3′-((1-(*p*-Tolyl)-1*H*-1,2,3-triazol-4-yl)methylene)bis(4-hydroxy-2*H*-chromen-2-one) (**6b**) The compound **6b** was prepared according to general procedure from aldehyde **4b** and 4-hydroxycoumarin **5**, in 82% yield. Mp 166–168 °C. IR *v* max/cm^{-1} 3314, 3065, 1659, 1614, 1565, 760. ^{1}H NMR (400 MHz, $CDCl_3$) δ 8.06–7.86 (*m*, 3H), 7.56–7.41 (*m*, 4H), 7.35–7.05 (*m*, 6H), 6.27 (*s*, 1H), 2.36 (*s*, 3H). ^{13}C NMR (100 MHz, $CDCl_3$) δ 170.1, 167.8, 167.7, 164.5, 152.4, 138.9, 137.6, 134.5, 132.5, 130.0, 124.4, 120.6, 120.4, 116.4, 103.7, 30.2, 21.1.

3,3′-((1-(2-Methoxyphenyl)-1*H*-1,2,3-triazol-4-yl)methylene)bis(4-hydroxy-2*H*-chromen-2-one) (**6c**) The compound **6c** was prepared according to general procedure from aldehyde **4c** and 4-hydroxycoumarin **5**, in 80% yield. Mp

above 270 °C. IR *v* max/cm^{-1} 3397, 1650, 1606, 1534, 756. ^{1}H NMR (400 MHz, DMSO-d_6) δ 8.06 (*s*, 1H), 7.89 (*d*, *J* = 7.6 Hz, 2H), 7.86 (*s*, 1H), 7.62 (*d*, *J* = 7.7 Hz, 1H), 7.49–7.40 (*m*, 3H), 7.22 (*d*, *J* = 6.9 Hz, 3H), 7.16 (*d*, *J* = 8.2 Hz, 1H), 7.08 (*t*, *J* = 7.5 Hz, 1H), 6.45 (*s*, 1H), 3.82 (*s*, 3H). ^{13}C NMR (100 MHz, $CDCl_3$ + DMSO-d_6) δ 168.3, 164.9, 152.5, 151.1, 147.9, 130.8, 129.8, 126.1, 125.1, 124.2, 123.9, 122.8, 120.7, 120.0, 115.4, 112.6, 103.1, 55.9, 29.4. HRMS (ESI-TOF, $[M + H]^+$): *m*/*z* calcd for $C_{28}H_{19}N_3O_7$, 510.1301; found, 510.1296.

3,3′-((1-(4-Methoxyphenyl)-1*H*-1,2,3-triazol-4-yl)methylene)bis(4-hydroxy-2*H*-chromen-2-one) (**6d**) The compound **6d** was prepared according to general procedure from aldehyde **4d** and 4-hydroxycoumarin **5**, in 90% yield. Mp 170–172 °C. IR *v* max/cm^{-1} 3462, 3076, 1657, 1610, 762. ^{1}H NMR (400 MHz, $CDCl_3$) δ 7.99 (*s*, 2H), 7.86 (*s*, 1H), 7.71–7.48 (*m*, 4H), 7.40–7.14 (*m*, 4H), 6.94 (*s*, 2H), 6.22 (*s*, 1H), 3.83 (*s*, 3H). ^{13}C NMR (100 MHz, $CDCl_3$) δ 167.8, 167.7, 159.8, 152.4, 132.8, 132.7, 130.3, 124.6, 124.4, 122.1, 120.8, 117.1, 116.5, 114.6, 103.9, 55.6, 30.4.

3,3′-((1-(2-Chlorophenyl)-1*H*-1,2,3-triazol-4-yl)methylene)bis(4-hydroxy-2*H*-chromen-2-one) (**6e**) The compound **6e** was prepared according to general procedure from aldehyde **4e** and 4-hydroxycoumarin **5**, in 82% yield. Mp 146–148 °C. IR *v* max/cm^{-1} 3338, 1653, 1604, 1540, 754. ^{1}H NMR (400 MHz, DMSO-d_6) δ 8.01 (*s*, 1H), 7.97 (*d*, *J* = 5.4 Hz, 2H), 7.63–7.61 (*m*, 2H), 7.57–7.49 (*m*, 4H), 7.31–7.28 (*m*, 4H), 6.53 (*s*, 1H). ^{13}C NMR (100 MHz, $CDCl_3$) δ 172.1, 165.9, 165.1, 152.4, 144.3, 142.5, 134.8, 132.5, 130.7, 130.6, 128.7, 127.8, 126.1, 124.6, 124.5, 116.5, 103.8, 30.2. HRMS (ESI-TOF, $[M + H]^+$): *m*/*z* calcd for $C_{27}H_{16}ClN_3O_6$, 514.0806; found, 514.0804.

3,3′-((1-(3-Chlorophenyl)-1*H*-1,2,3-triazol-4-yl)methylene)bis(4-hydroxy-2*H*-chromen-2-one) (**6f**) The compound **6f** was prepared according to general procedure from aldehyde **4f** and 4-hydroxycoumarin **5**, in 86% yield. Mp 188–190 °C. IR *v* max/cm^{-1} 3482, 3175, 1654, 1606, 760. ^{1}H NMR (400 MHz, DMSO-d_6) δ 8.21 (*s*, 1H), 8.05 (*s*, 1H), 7.93 (*s*, 1H), 7.89 (*d*, *J* = 8.1 Hz, 2H), 7.81 (*d*, *J* = 8.1 Hz, 1H), 7.47 (*d*, *J* = 8.0 Hz, 2H), 7.37 (*d*, *J* = 8.0 Hz, 1H), 7.21 (*d*, *J* = 7.7 Hz, 4H), 6.43 (*s*, 1H). ^{13}C NMR (100 MHz, $CDCl_3$ + DMSO-d_6) δ 168.4, 165.1, 152.9, 150.2, 138.3, 134.7, 131.3, 130.9, 127.9, 124.6, 122.9, 120.5, 120.5, 119.8, 118.3, 115.7, 103.2, 29.8. HRMS (ESI-TOF, $[M + H]^+$): *m*/*z* calcd for $C_{27}H_{16}ClN_3O_6$, 514.0806; found, 514.0804.

3,3′-((1-(4-Chlorophenyl)-1*H*-1,2,3-triazol-4-yl)methylene)bis(4-hydroxy-2*H*-chromen-2-one) (**6g**) The compound **6g** was prepared according to general procedure from aldehyde **4g** and 4-hydroxycoumarin **5**, in 88% yield. Mp 204–206 °C. IR *v* max/cm^{-1} 3341, 1605, 1547, 755. ^{1}H NMR (400 MHz, $CDCl_3$) δ 7.99 (*s*, 4H), 7.89 (*s*, 1H), 7.62 (*s*, 4H), 7.42 (*s*, 2H), 7.35 (*s*, 2H), 6.20 (*s*, 1H). ^{13}C NMR (100 MHz, $CDCl_3$) δ 190.5, 167.9, 165.7, 152.4, 144.9, 135.3, 134.6, 133.0, 129.9, 124.8, 124.5, 121.7, 120.5, 116.6, 103.7, 30.4. HRMS (ESI-TOF, $[M + H]^+$): *m*/*z* calcd for $C_{27}H_{16}ClN_3O_6$, 514.0806; found, 514.0799.

3,3′-((1-(3-Bromophenyl)-1*H*-1,2,3-triazol-4-yl)methylene)bis(4-hydroxy-2*H*-chromen-2-one) (**6h**) The compound **6h** was prepared according to general procedure from aldehyde **4h** and 4-hydroxycoumarin **5**, in 80% yield. Mp 205–206 °C. IR *v* max/cm^{-1} 3118, 1654, 1606, 755. ^{1}H NMR (400 MHz, $CDCl_3$) δ 11.66 (*s*, 2H), 8.04 (*d*, *J* = 7.9 Hz, 2H), 7.89 (*d*, *J* = 11.4 Hz, 2H), 7.71 (*d*, *J* = 7.4 Hz, 1H), 7.63 (*t*, *J* = 7.4 Hz, 2H), 7.56 (*d*, *J* = 7.7 Hz, 1H), 7.41–7.36 (*m*, 5H), 6.14 (*s*, 1H). ^{13}C NMR (100 MHz, $CDCl_3$) δ 168.0, 167.9, 165.2, 152.5, 144.8, 137.9, 133.2, 131.9, 131.1, 125.0, 124.5, 123.6, 123.3, 120.3, 119.2, 116.7, 103.9, 30.6. HRMS (ESI-TOF, $[M + H]^+$): *m*/*z* calcd for $C_{27}H_{16}BrN_3O_6$, 558.0300; found, 558.0295.

3,3′-((1-(2-Nitrophenyl)-1*H*-1,2,3-triazol-4-yl)methylene)bis(4-hydroxy-2*H*-chromen-2-one) (**6i**) The compound **6i** was prepared according to general procedure from aldehyde **4i** and 4-hydroxycoumarin **5**, in 86% yield. Mp 180–182 °C. IR *v* max/cm^{-1} 3361, 1648, 1533, 755. ^{1}H NMR (400 MHz, $CDCl_3$) δ 11.79 (*s*, 2H), 8.09 (*d*, *J* = 8.1 Hz, 1H), 8.04 (*d*, *J* = 7.9 Hz, 2H), 7.80 (*t*, *J* = 7.1 Hz, 1H), 7.75 (*s*, 1H), 7.70 (*t*, *J* = 6.8 Hz, 2H), 7.63 (*t*, *J* = 7.1 Hz, 2H), 7.43–7.37 (*m*, 4H), 6.19 (*s*, 1H). ^{13}C NMR (100 MHz, $CDCl_3$) δ 190.7, 165.2, 163.8, 152.5, 144.5, 133.9, 133.1, 130.9, 130.3, 128.4, 125.7, 125.0, 124.5, 124.0, 119.9, 116.7, 104.0, 30.6. HRMS (ESI-TOF, $[M + H]^+$): *m*/*z* calcd for $C_{27}H_{16}N_4O_8$, 525.1046; found, 525.1048.

3,3′-((1-(3-Nitrophenyl)-1*H*-1,2,3-triazol-4-yl)methylene)bis(4-hydroxy-2*H*-chromen-2-one) (**6j**) The compound **6j** was prepared according to general procedure from aldehyde **4j** and 4-hydroxycoumarin **5**, in 85% yield. Mp 180–183 °C. IR *v* max/cm^{-1} 3389, 1658, 1610, 757. ^{1}H NMR (400 MHz, DMSO-d_6) δ 8.73 (*s*, 1H), 8.59 (*s*, 1H), 8.36 (*s*, 1H), 8.22 (*s*, 1H), 7.92 (*d*, *J* = 7.4 Hz, 2H), 7.79 (*t*, *J* = 8.0 Hz, 1H), 7.53 (*s*, 2H), 7.27 (*d*, *J* = 9.5 Hz, 3H), 7.04 (*s*, 1H), 6.46 (*s*, 1H). ^{13}C NMR (100 MHz, $CDCl_3$ + DMSO-d_6) δ 166.9, 164.8, 152.5, 149.3, 148.5, 137.6, 131.2, 131.1, 125.5, 124.2, 123.1, 122.2, 120.7, 119.2, 115.6, 114.2, 102.9, 29.5.

3,3′-((1-(4-Nitrophenyl)-1*H*-1,2,3-triazol-4-yl)methylene)bis(4-hydroxy-2*H*-chromen-2-one) (**6k**) The compound **6k** was prepared according to general procedure from aldehyde **4k** and 4-hydroxycoumarin **5**, in 80% yield. Mp 204–206 °C. IR *v* max/cm^{-1} 3400, 1602, 749. ^{1}H NMR (400 MHz, $CDCl_3$) δ 11.68 (*s*, 2H), 8.40 (*d*, *J* = 8.0 Hz, 2H), 8.05 (*d*, *J* = 8 Hz, 2H), 7.97 (*d*, *J* = 8 Hz, 3H), 7.65 (*t*, *J* = 8 Hz, 2H), 7.41 (*t*, *J* = 8.2 Hz, 4H), 6.16 (*s*, 1H). ^{13}C NMR (100 MHz, $CDCl_3$) δ 168.1, 165.2, 152.5, 147.2, 146.9, 145.4, 141.1, 133.2, 125.5, 125.1, 124.4, 120.5, 120.1, 116.7, 103.8, 30.6. HRMS (ESI-TOF, $[M + H]^+$): *m*/*z* calcd for $C_{27}H_{16}N_4O_8$, 525.1046; found, 525.1060.

Pharmacology

Antitubercular activity

All the chemicals such as sodium salt XTT and MTT, DMSO and rifampicin were purchased from Sigma-Aldrich, USA. Synthesized compounds were dissolved in DMSO and it was used as a stock solution (10 mg/mL) for further biological testing.

A microbial strain, *Mtb* H37Ra (ATCC 25177), was obtained from Astra Zeneca, India. The stock culture was maintained at − 80 °C and subcultured once in a liquid medium before inoculation into an experimental culture. For the antitubercular assay, *M. pheli* medium (minimal essential medium) was used. It contains 0.5 g KH_2PO_4, 0.25 g trisodium citrate, 60 mg $MgSO_4$, 0.5 g asparagine and 2 mL glycerol in distilled water (100 mL) followed by pH adjustment to 6.6. It takes at least 8–10 days for OD 1 at 620 nm. The antitubercular assay was performed in 96-well plates for the active as well as the dormant stages. All the synthetic compounds were screened for their in vitro activity against *Mycobacterium tuberculosis* H37Ra (ATCC 25177) using dilutions ranging from 20 to 0.625 μg/mL, in order to determine the actual minimum inhibitory concentration (MIC). The screening of *M. tuberculosis* H37Ra has been carried out by XTT Reduction Menadione Assay (XRMA) by reading absorbance at 470 nm. The optical density was read on a micro-plate reader with a 470-nm filter for XTT against a blank prepared from cell-free wells. Absorbance given by cells treated with the vehicle (DMSO) alone was taken as 100% cell growth. Initially, primary screening was carried out at 20, 10 and 5 μg/mL. Compounds showing more inhibition of MTB at or lower than 20 μg/mL were selected for further dose response curves. All the experiments were performed in duplicate and the quantitative value was expressed as the average ± standard deviation. MIC and IC_{50} values of the selected compounds were calculated from their dose response curves by using Origin 8 software. Percentage inhibition was calculated using the formula: $\%\text{inhibition} = [(\text{control} - \text{CMP})/(\text{control} - \text{blank})] \times 100$ where 'control' is the activity of *Mycobacterium* without compounds, 'CMP' is the activity of the *Mycobacterium* in the presence of compounds and 'blank' is the activity of the culture medium without *Mycobacterium*.

1,1-Diphenyl-1-picrylhydrazyl radical scavenging activity

The bleaching of the purple-colored methanol solution of DPPH radical scavenging activity was used for the determination of the hydrogen atoms or electron donation ability of the compounds. The stable radical DPPH was used as a reagent in spectrophotometric assay. Next, 1 mL of various concentrations of the test compounds (5, 10, 25, 50 and 100 μg/mL) in methanol was added to 4 mL of 0.004% (w/v) methanol solution of DPPH. After a 30-min incubation period at room temperature, the absorbance was measured against blank at 517 nm. The percent inhibition (I%) of free radical production from DPPH was calculated by the following equation:

$$\%\text{ of scavenging} = [(\text{A control} - \text{A sample})/\text{A blank}] \times 100$$

where "A control" is the absorbance of the control reaction (containing all reagents except the test compound) and "A sample" is the absorbance of the test compound. Tests were carried out in triplicate.

Molecular docking studies

To study the binding mode of the title compounds into the active site of the DprE1 enzyme, the Grid-Based Ligand Docking with Energetics (GLIDE) module integrated in the Small Drug Discovery Suite of the Schrodinger molecular modeling software [67] was used. It involved mainly enzyme selection and preparation, receptor grid generation, ligand building and preparation, and docking and analysis of docking studies. With this purpose, the three-dimensional X-ray structure of *M. tuberculosis* DprE1 (Accession number 4FDO) in complex with its inhibitor was retrieved from the Protein Data Bank. The protein structure was prepared for docking simulation using the Protein Preparation Wizard which involved removing the crystallographically observed water molecules (as none of them was found to be conserved in the interaction with the protein), and adding the missing hydrogen/side chain atoms corresponding to pH 7.0 which was considered the appropriate ionization state for the acidic as well as the basic amino acid residues. After assigning appropriate charge and protonation states to the obtained structure, the energy minimization with a root mean square deviation (RMSD) value of 0.30 Å was then carried out using the OPLS-2005 force field to relieve the steric clashes between the residues caused due to the addition of hydrogen atoms and this structure was used for further docking studies. Molecules to be docked were drawn in 3D form with the *build* panel in Maestro and refined by the *LigPrep* module. The molecules were subjected to the OPLS-2005 force field which involves addition of hydrogen, adjusting realistic bond lengths and angles, correct chiralities, ionization states, tautomers, stereo chemistries and ring conformations and assigning partial charges. The ligand structures thus obtained were finally optimized by energy minimization until it reached a RMSD cutoff of 0.01 Å. The active site of DprE1 for docking was defined using the *Receptor Grid Generation* panel in Glide. A grid box of 12 × 12 × 12 Å dimensions centered on the centroid of the native ligand in the crystal complex was generated which was sufficient to explore a larger region of the enzyme structure. The co-crystallized ligand serves as the reference coordinate signifying the active site for an inhibitor molecule with respect to the biological target. The optimized ligand structures were then subjected to docking calculation against the defined active site using the *extra precision* (i.e., GlideXP) scoring function to rank the docking poses and to gauge their binding affinities towards the DprE1 enzyme. The output files generated in the form of the docking poses were visualized and analyzed using the Maestro's Pose Viewer utility for the key elements of interaction with the active site residues.

Results and discussion

Chemistry

The synthetic route for the designed 1,2,3-triazole-incorporated biscoumarin conjugates using the molecular hybridization approach has been depicted in Scheme 1. The commercially available anilines **1a–k** were successively diazotized

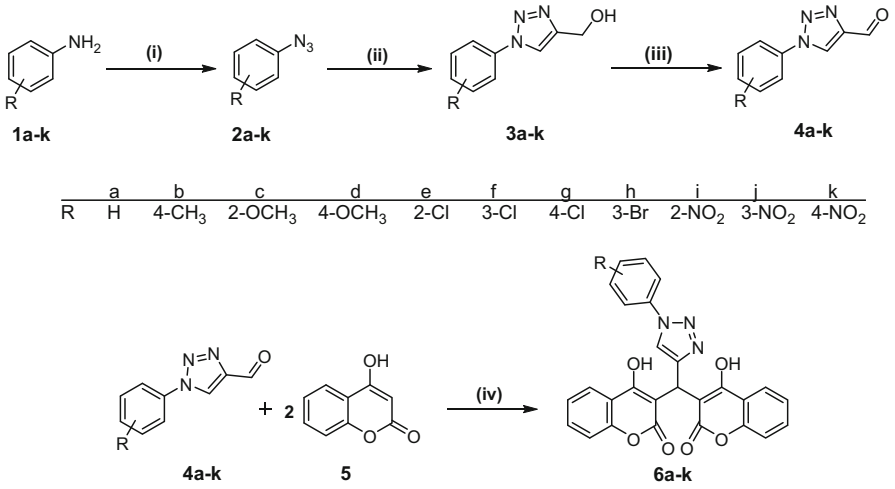

Scheme 1 Synthetic route for 1,2,3-triazole-incorporated biscoumarin conjugates

followed by treatment with sodium azide resulting in the corresponding aryl azides **2a**–**k**. The aryl azides **2a**–**k** on 1,3-dipolar cycloaddition reaction (click reaction) with propargyl alcohol using copper sulfate and sodium ascorbate in *t*-butanol:H_2O, resulted in 1,4-disubstituted 1,2,3-triazolyl methanols **3a**–**k** in quantitative yields. The triazolyl methanols **3a**–**k** were subjected to oxidation using Collins reagent (CrO_3:2Py) in dichloromethane affording the corresponding triazolyl aldehydes **4a**–**k** in 55–65% isolated yield. The 1,2,3-triazolyl aldehydes **4a**–**k** on reaction with commercially available 4-hydroxycoumarin in ethanol and acetic acid resulted in the corresponding 1,2,3-triazole-incorporated biscoumarin conjugates **6a**–**k** in 80–90% yield (Scheme 1). The structures of all the conjugates were confirmed by physical data and spectral analysis. In the ^{1}H NMR spectra for all the conjugates,

Reagents and conditions: (1) $NaNO_2$, HCl, 0 °C; NaN_3, 2–4 h, rt; (2) propargyl alcohol, $CuSO_4$, sodium ascorbate, *t*-butanol:H_2O (1:1), 48–72 h, rt; (3) CrO_3:2Py, CH_2Cl_2, 3–6 h, rt; (4) EtOH–AcOH, reflux, 4–6 h.

The singlet signal observed at δ 7.98–8.30 ppm was assigned to the triazole proton. The other prominent singlet signal was observed at δ 6.12–6.55 ppm and assigned to the methine proton. In the ^{13}C NMR spectra for all conjugates, the signals appeared at δ 29–31 ppm, and were assigned for methine carbon.

Biological activity

Antitubercular activity

The newly synthesized compounds **6a**–**k** were initially screened for their in vitro antitubercular activity against *M. tuberculosis* H37Ra (ATCC 25177) at three different concentrations, 20, 10 and 5 μg/mL, using an established XRMA [68] screening protocol, and the results are displayed in supplementary information

(Table S1). Rifampicin was used as the reference drug. Among the screened compounds, **6b**, **6c**, **6e**, **6f**, **6g**, **6h** and **6k** showed more than 77.84% inhibition towards *Mtb* H37Ra which supports the antimicrobial nature of the biscoumarin hybrids. The compounds were further evaluated in secondary screening at six different concentrations, 20, 10, 5, 2.5, 1.25 and 0.625, in order to determine the actual MIC. The obtained results of the screening are tabulated in Table 1.

Structure–activity relationship

The antitubercular activity was significantly affected by introducing various substituents on the phenyl ring. Among the compounds **6a–k**, compound **6h** (R = 3-Br) showed good antitubercular activity with an IC_{50} value of 1.44 μg/mL against dormant *Mtb* H37Ra. Compounds **6f** (R = 3-Cl) and **6g** (R = 4-Cl) showed good antitubercular activity against dormant *Mtb* H37Ra with IC_{50} values of 8.27 and 6.27 μg/mL, respectively. Compounds **6a**, **6b**, **6c**, **6d**, **6e**, **6i** and **6k** having substituents R = H, 4-CH_3, 2-OCH_3, 4-OCH_3, 2-Cl, 2-NO_2 and 4-NO_2 showed moderate antitubercular activity against dormant *Mtb* H37Ra with IC_{50} values of 13.1, 12.28, 14.28, 19.45, 10.42, 20.00 and 13.12 μg/mL, respectively. Hence, among all the compounds **6a–k**, the derivatives **6a**, **6b**, **6c**, **6d**, **6e**, **6f**, **6g**, **6h**, **6i** and **6k** showed good to moderate antitubercular activity against dormant *Mtb* H37Ra (Table 1).

Compounds **6g** and **6h** showed good antitubercular activity against active *Mtb* H37Ra with IC_{50} values of 7.48 and 1.93 μg/mL, respectively. Compounds **6a**, **6b**, **6c**, **6e**, **6f** and **6k** showed moderate antitubercular activity against active *Mtb* H37Ra with IC_{50} values of 15.64, 13.81, 15.17, 11.38, 10.00 and 14.38 μg/mL, respectively. Hence, among all the compounds, the hybrids **6a**, **6b**, **6c**, **6e**, **6f**, **6g**, **6h** and **6k** showed good to moderate antitubercular activity against active *Mtb* H37Ra (Table 1). The presence of –CH_3, –OCH_3, –Cl, –Br and –NO_2 groups on the phenyl ring largely influence the antitubercular activity in the dormant and active states of *Mtb* H37Ra. The electron-donating as well as electron-withdrawing groups is responsible for antitubercular activity. The halogen groups are also responsible for the antitubercular activity.

Anti-oxidant activity

Triazole–biscoumarin conjugates were evaluated for their in vitro free radical scavenging activity. The anti-oxidant activity of compounds **6a–k** resulted by using the DPPH radical scavenging assay and the results are summarized in Table 1. Butylated hydroxytoluene (BHT) was used as the standard drug having an IC_{50} value of 16.47 ± 0.18 μg/mL. All the synthesized compounds showed excellent anti-oxidant activity compared with BHT, except for **6e.** Compound **6b** showed excellent anti-oxidant activity with an IC_{50} value of 8.17 ± 0.11 μg/mL and compounds **6j** and **6g** exhibited excellent anti-oxidant activity with IC_{50} values of 8.44 ± 0.64 and 9.15 ± 0.34 μg/mL, respectively. This shows that theompounds **6b**, **6j** and **6g** are highly active copmared with the standard BHT drug. Compounds **6k**, **6d**, **6c** and **6f** exhibited excellent anti-oxidant activity with IC_{50} values of

Table 1 In vitro antitubercular and anti-oxidant activities of triazole-biscoumarin conjugate **6a–k**

Entry		*M. tuberculosis* H37Ra (μg/mL)				DPPH IC_{50} (μg/mL)
		Active		Dormant		
		IC_{50}	IC_{90}	IC_{50}	IC_{90}	
6a	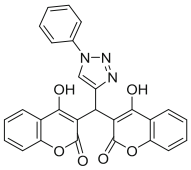	15.64	> 20	13.1	> 20	15.23 ± 0.34
6b	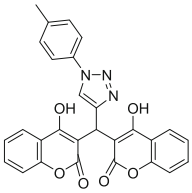	13.81	> 20	12.28	> 20	08.17 ± 0.11
6c	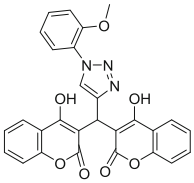	15.17	> 20	14.28	> 20	12.94 ± 0.05
6d	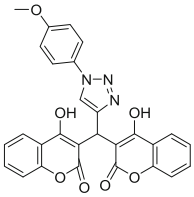	–	–	19.45	> 20	11.64 ± 0.09
6e	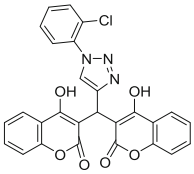	11.38	> 20	10.42	> 20	18.22 ± 0.34
6f	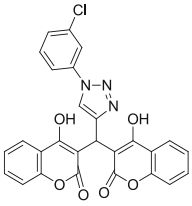	10.00	> 20	8.27	20.00	13.33 ± 0.47

Table 1 continued

Entry		*M. tuberculosis* H37Ra (μg/mL)				DPPH IC_{50} (μg/mL)
		Active		Dormant		
		IC_{50}	IC_{90}	IC_{50}	IC_{90}	
6g	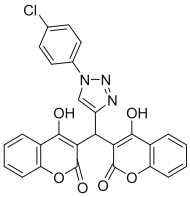	7.48	17.5	6.27	16.75	09.15 ± 0.34
6h	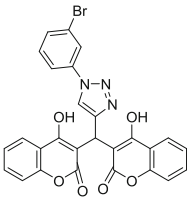	1.93	15.13	1.44	9.99	16.13 ± 0.87
6i	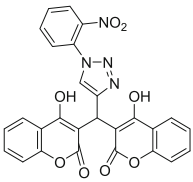	–	–	20.00	> 20	14.08 ± 0.78
6j	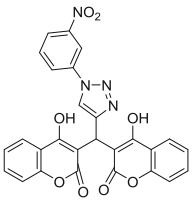	–	–	–	–	08.44 ± 0.64
6k	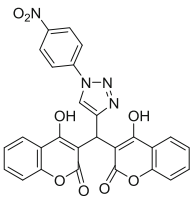	14.38	> 20	13.12	> 20	11.15 ± 0.76
RIF	–	0.020	0.53	0.0019	0.80	–
BHT	–	–	–	–	–	16.47 ± 0.18

RIF rifampicin, *BHT* butylated hydroxy toluene, *DPPH* 2,2-diphenyl-1-picrylhydrazyl, – not calculated

11.15 ± 0.76, 11.64 ± 0.09, 12.94 ± 0.05 and 13.33 ± 0.47 μg/mL, respectively. Compounds **6i**, **6a** and **6h** showed anti-oxidant activity close to the standard drug with IC_{50} values of 14.08 ± 0.78, 15.23 ± 0.34 and 16.13 ± 0.87 μg/mL, respectively (Table 1).

Computational study

Molecular docking

In an effort to gain a better understanding of the potency of the 1,2,3-triazole–coumarin conjugates and to elucidate the mechanism by which the compounds can induce antitubercular activity. A molecular docking study was performed into the binding site of DprE1 for the triazole–coumarin conjugates. The DprE1 enzyme is one of the most vulnerable targets of *M. tuberculosis*. It is an oxidase enzyme involved in arabinogalactan biosynthesis (cell wall biogenesis), shown to be a crucial target for the survival of *M. tuberculosis*. It is a key enzyme in the biosynthesis of the basic precursor for the mycobacterial cell wall core decaprenylphosphoryl-D-arabinose, the only known donor of D-arabinofuranosyl residues for the synthesis of arabinogalactan.

Results from the ensuing docking simulation revealed that the 1,2,3-triazole–coumarin conjugates bind well to the active site of DprE1 by the formation of several bonded and non-bonded interactions, occupying coordinates very close to that of the native ligand with a varying magnitude of affinity. The docking score for the most active compound, **6h**, is − 8.935, while for the least active, **6j**, it is − 6.147. These theoretical predictions were in agreement with the experimental antitubercular activity, the most active compounds exhibiting higher docking scores while those with relatively least activity having a lower docking score. Further, a detailed per-residual interaction analysis has been performed to gain an insight into the thermodynamic elements governing the binding event of these molecules through which we can speculate the binding patterns in the active site. The lowest energy docked conformation of **6h** was observed to be tightly bound to the active site of DprE1, engaging in a series of steric and electrostatic interactions (Fig. 4).

These interactions contributed to the highest binding affinity observed for **6h**. The per-residue interaction analysis shows that the compound is stabilized in the active site through significant van der Waals interactions with Lys418 (− 3.561 kcal/mol), Csy387 (− 2.859 kcal/mol), Asn385 (− 1.481 kcal/mol),

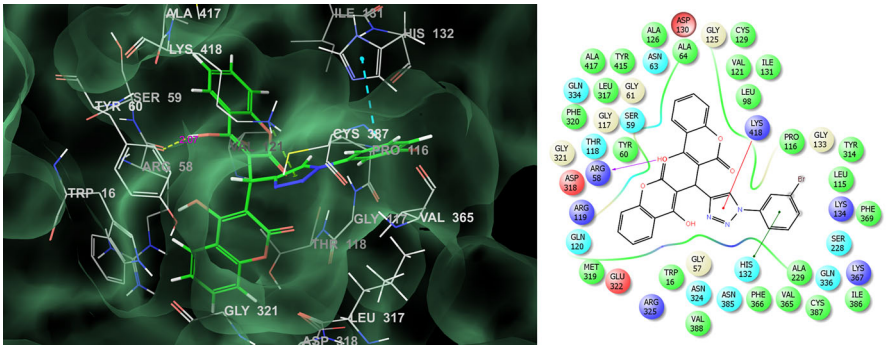

Fig. 4 Binding mode of **6h** into the active site of DprE1 (right side: green lines signify π–π stacking interactions while the pink lines represent the hydrogen bonding interactions)

Lys367 (− 2.459 kcal/mol), Val365 (− 2.964 kcal/mol), Leu363 (− 1.523 kcal/mol), Gln336 (− 1.921 kcal/mol), His132 (− 3.559 kcal/mol), and Pro116 (− 4.141 kcal/mol) residues via its 1-(3-bromophenyl)-1*H*-1,2,3-triazol-4-yl scaffold, while the 4-hydroxy-2*H*-chromen-2-one component became engaged in similar types of interactions with Ala417 (− 2.316 kcal/mol), Tyr415 (− 2.863 kcal/mol), Gly321 (− 1.984 kcal/mol), Phe320 (− 2.263 kcal/mol), Asp318 (− 2.929 kcal/mol), Leu317 (− 3.259 kcal/mol), Csy129 (− 1.942 kcal/mol), Val121 (− 1.888 kcal/mol), Thr118 (− 3.513 kcal/mol), Gly117 (− 4.667 kcal/mol), Tyr60 (− 2.749 kcal/mol), Ser59 (− 1.967 kcal/mol), Arg58 (− 4.122 kcal/mol), Trpand 16 (− 2.063 kcal/mol) lining the active site of DprE1. The high affinity observed for **6h** is also attributed to the electrostatic interactions shown by **6h** with Lys418 (− 11.452 kcal/mol), Lys367 (− 2.039 kcal/mol), Glu322 (− 2.908 kcal/mol), Lys134 (− 1.974 kcal/mol), and Trp16 (− 1.495 kcal/mol) residues. The non-bonded interactions were seen to be the principal driving force for anchoring the **6h** to the enzyme cavity. Furthermore, binding is stabilized by one hydrogen bond and two π stacking (π–π and π–cation interactions). The hydroxyl group of the coumarin ring formed a crucial hydrogen bond with the carbonyl oxygen of Arg58 with a bonding distance of 2.07 Å. One π–π stacking interaction was observed between the bromo-phenyl ring and His132, while a π–cation interaction was observed for the triazole ring and Lys418 with bonding distances of 2.771 and 2.479 further stabilizing the ligand–enzyme complex. Such bonding interactions serve as an anchor guiding the 3D orientation of the ligand in the active pocket and further facilitate the non-bonded (steric and electrostatic) interactions.

A similar binding mode and network of interaction were also observed for **6a** (Fig. 5), **6b** (Fig. 6), **6c** (Fig. 7), **6d** (Fig. 8), **6e** (Fig. 9), **6f** (Fig. 10), **6g** (Fig. 11), **6i** (Fig. 12), **6j** (Fig. 13) and **6k** (Fig. 14), but diminishing regularly with observed antitubercular activity. Comparing the results of **6h** with the least active analogue, **6j**, revealed that this compound was as well bound to the active site of DprE1 at the same coordinate as **6h**, engaging in a very similar network of non-bonded and

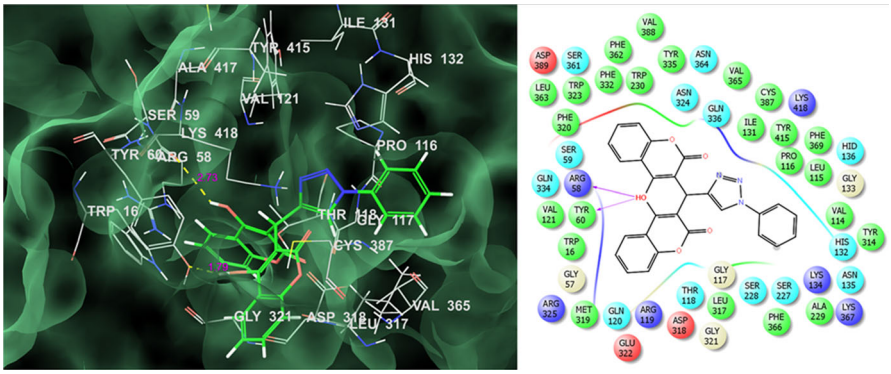

Fig. 5 Binding mode of **6a** into the active site of DprE1 (right side: green lines signify π–π stacking interactions while the pink lines represent the hydrogen bonding interactions)

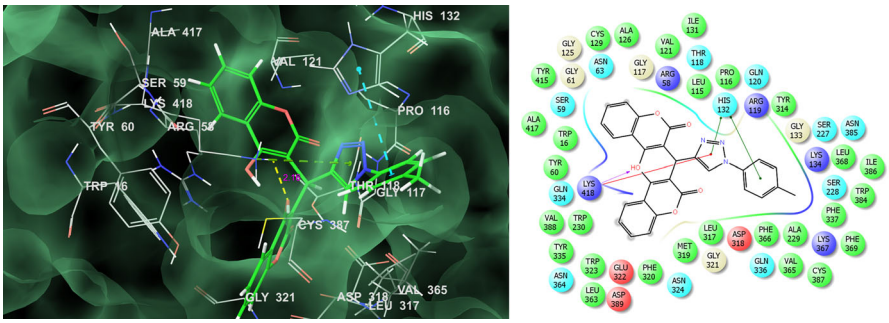

Fig. 6 Binding mode of **6b** into the active site of DprE1 (right side: green lines signify π–π stacking interactions while the pink lines represent the hydrogen bonding interactions)

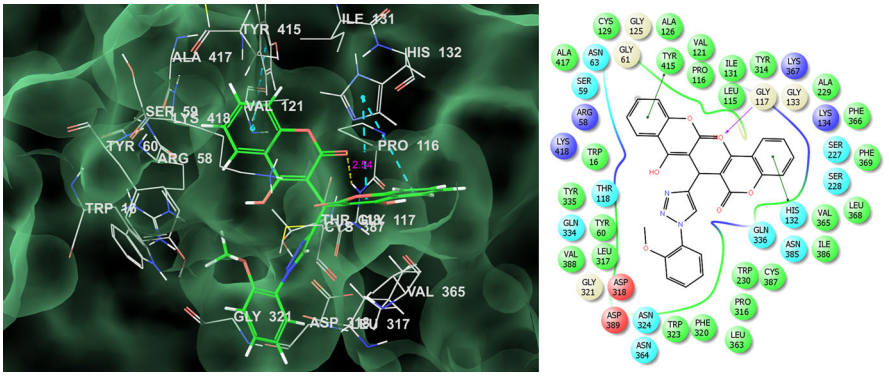

Fig. 7 Binding mode of **6c** into the active site of DprE1 (right side: green lines signify π–π stacking interactions while the pink lines represent the hydrogen bonding interactions)

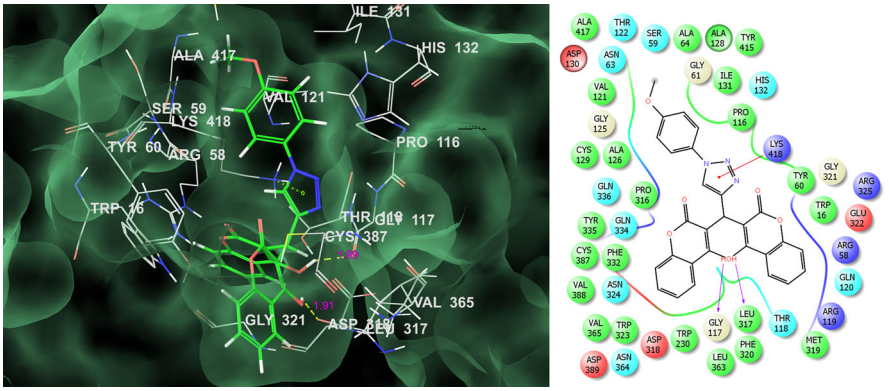

Fig. 8 Binding mode of **6d** into the active site of DprE1 (right side: green lines signify π–π stacking interactions while the pink lines represent the hydrogen bonding interactions)

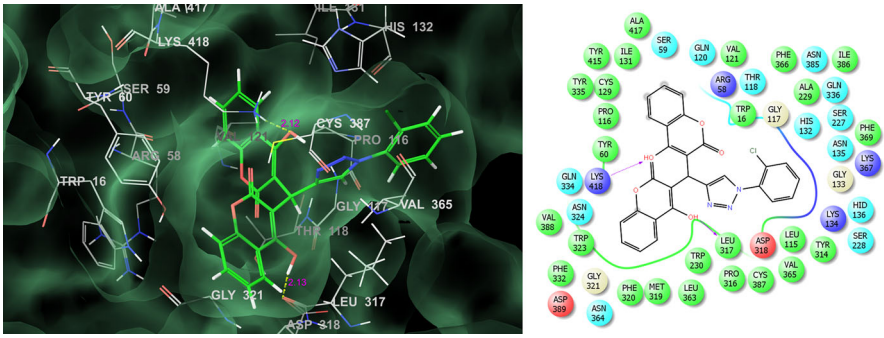

Fig. 9 Binding mode of **6e** into the active site of DprE1 (right side: green lines signify π–π stacking interactions while the pink lines represent the hydrogen bonding interactions)

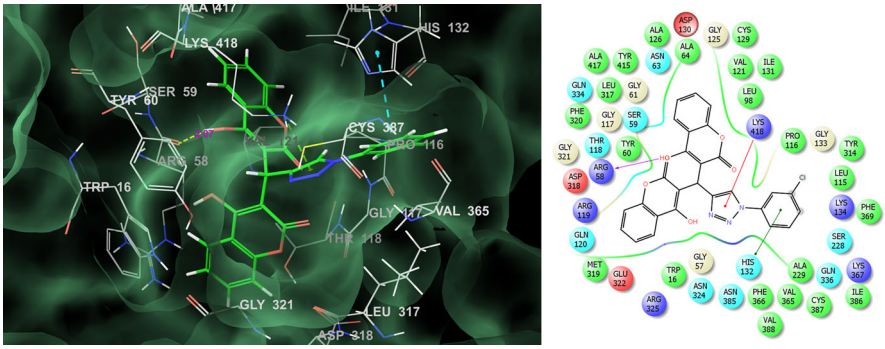

Fig. 10 Binding mode of **6f** into the active site of DprE1 (right side: green lines signify π–π stacking interactions while the pink lines represent the hydrogen bonding interactions)

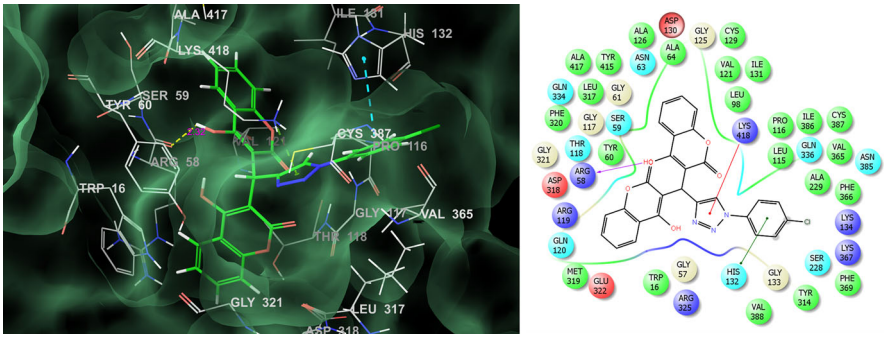

Fig. 11 Binding mode of **6g** into the active site of DprE1 (right side: green lines signify π–π stacking interactions while the pink lines represent the hydrogen bonding interactions)

bonded interactions (H-bond and π stacking). However, it is noteworthy that the per-residue interactions observed for **6j** were significantly lower than for **6h**, which could be the fundamental cause for the weaker binding affinity observed for **6j**,

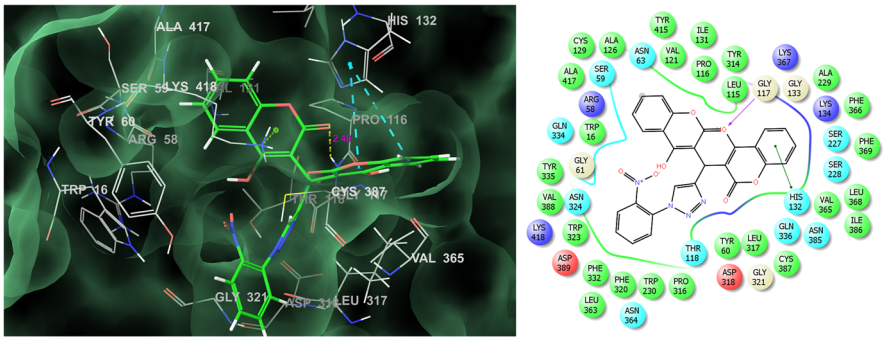

Fig. 12 Binding mode of **6i** into the active site of DprE1 (right side: green lines signify π–π stacking interactions while the pink lines represent the hydrogen bonding interactions)

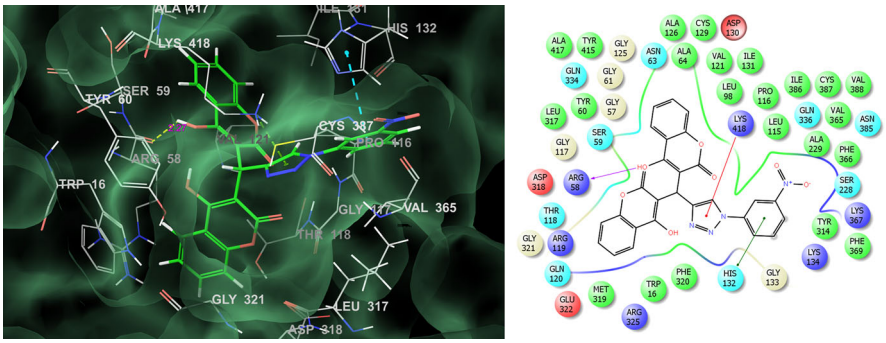

Fig. 13 Binding mode of **6j** into the active site of DprE1 (right side: green lines signify π–π stacking interactions while the pink lines represent the hydrogen bonding interactions)

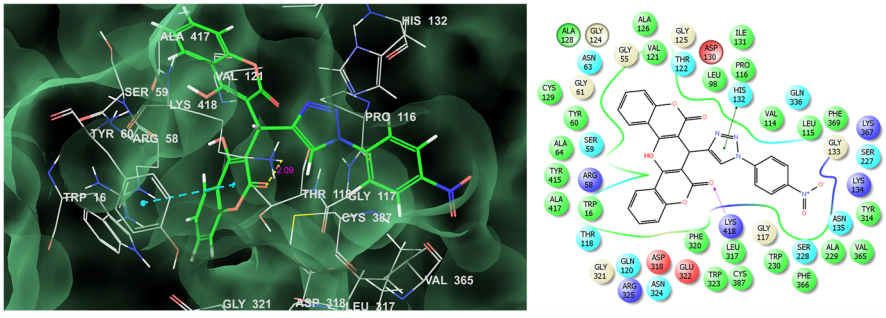

Fig. 14 Binding mode of **6k** into the active site of DprE1 (right side: green lines signify π–π stacking interactions while the pink lines represent the hydrogen bonding interactions)

which is in agreement with the experimental antitubercular activity. For the sake of brevity of text, the detailed per-residue interaction analyses for other compounds and binding modes are given in Table 2. Overall, it is evident from the docking studies that the compounds possess a promising affinity for this crucial

Table 2 Quantitative per-residue interaction analysis of the molecular docking study on DprE1 for the most active triazole–biscoumarin conjugate analogues

Entry	Docking score	Glide interaction energy (kcal/mol)	Per-residues interactions			
			Van der Waals (kcal/mol)	Coulombic (kcal/mol)	H-bonds (Å)	π–π/π–cation stacking (Å)
6a	− 7.271	− 44.796	Lys418 (− 2.626), Ala417 (− 1.863), Tyr415 (− 1.946), Asp389 (− 1.483), Csy387 (− 1.881), Val365 (− 1.544), Leu363 (− 1.211), Asn324 (− 1.421), Gly321 (− 1.629), Phe320 (− 1.279), Asp318 (− 1.771), Leu317 (− 2.657), Tyr314 (− 1.018), His132 (− 2.79), Thr118 (− 2.034), Gly117 (− 2.652), Pro116 (− 1.948), Tyr60 (− 1.946), Arg58 (− 1.582), Trp16 (− 2.071)	Lys418 (− 9.657), Asp389 (− 3.117), Asn324 (− 0.953), Glu322 (− 2.127), Gly117 (− 1.674), Pro116 (− 1.301), Tyr60 (− 3.271)	Arg58 (2.73), Tyr60 (1.79)	
6b	− 7.726	− 49.412	Lys418 (− 3.069), Ala417 (− 2.114), Tyr415 (− 2.014), Csy387 (− 2.133), Asn385 (− 1.143), Phe369 (− 1.214), Lys367 (− 1.669), Phe366 (− 1.198), Val365 (− 2.089), Leu363 (− 1.123), Gln336 (− 1.693), Gly321 (− 1.603), Phe320 (− 1.923), Leu317 (− 2.428), Tyr314 (− 1.011), His132 (− 1.363), Val121 (− 1.232), Thr118 (− 2.335), Gly117 (− 2.819), Pro116 (− 1.992), Tyr60 (− 2.098), Arg58 (− 2.294)	Lys418 (− 1.526), Asp389 (− 3.219), Arg119 (− 1.347), Pro116 (− 1.954)	Lys418 (2.16)	His132 (2.49)/ Lys418 (2.16)

Table 2 continued

Entry	Docking score	Glide interaction energy (kcal/mol)	Per-residues interactions			
			Van der Waals (kcal/mol)	Coulombic (kcal/mol)	H-bonds (Å)	π–π/π–cation stacking (Å)
6c	− 7.138	− 43.51	Lys418 (− 1.757), Ala417 (− 1.574), Tyr415 (− 1.911), Asp389 (− 1.382), Csy387 (− 1.753), Asn385 (− 1.643), Phe369 (− 1.165), Phe366 (− 1.082), Val365 (− 1.801), Leu363 (− 1.173), Gln336 (− 1.994), Asn324 (− 1.331), Gly321 (− 1.574), Phe320 (− 1.908), Leu317 (− 1.759), His132 (− 1.018), Ile131 (− 1.231), Thr118 (− 1.061), Gly117 (− 1.017), Pro116 (− 1.589), Tyr60 (− 1.337), Arg58 (− 1.259)	Lys418 (− 7.096), Asp389 (− 1.279), Arg119 (− 1.126), Arg58 (− 1.624)	Gly117 (2.54)	His132 (2.99), Tyr415 (1.81)
6d	− 6.869	− 40.573	Lys418 (− 1.681), Tyr415 (− 1.897), Csy387 (− 1.484), Leu363 (− 1.149), Asn324 (− 1.284), Glu322 (− 1.225), Gly321 (− 1.673), Phe320 (− 1.133), Asp318 (− 1.082), His132 (− 1.225), Csy129 (− 1.335), Val121 (− 1.602), 120 (− 1.348), Gly117 (− 1.294), Pro116 (− 1.614), Tyr60 (− 1.18), Ser59 (− 1.352), Arg58 (− 1.397), Trp16 (− 1.726)	Lys418 (− 5.091), Asp389 (− 1.446), Lys367 (− 1.146), Glu322 (− 2.057), Asp318 (− 3.099), Gly117 (− 2.8)	Gly117 (1.99), Leu317 (1.91)	Lys418 (2.274)

Table 2 continued

Entry	Docking score	Glide interaction energy (kcal/mol)	Per-residues interactions			
			Van der Waals (kcal/mol)	Coulombic (kcal/mol)	H-bonds (Å)	π–π/π–cation stacking (Å)
6e	− 7.909	− 50.278	Lys418 (− 3.276), Ala417 (− 2.154), Tyr415 (− 2.044), Asp389 (− 1.504), Csy387 (− 2.157), Asn385 (− 1.181), Phe369 (− 1.242), Lys367 (− 1.949), Val365 (− 2.198), Leu363 (− 1.316), Gln336 (− 1.725), Asn324 (− 1.211), Gly321 (− 1.806), Phe320 (− 2.149), Leu317 (− 2.518), Tyr314 (− 1.041), 228 (− 1.22), Lys134 (− 1.715), His132 (− 2.335), Val121 (− 1.257), Thr118 (− 3.123), Gly117 (− 3.625), Pro116 (− 2.935), Tyr60 (− 2.272), Arg58 (− 2.839)	Lys418 (− 6.834), Asp389 (− 1.132), Asp318 (− 1.327), Leu317 (− 1.307)	Lys418 (2.12), Leu317 (2.13)	–
6f	− 8.052	− 52.868	Lys418 (− 3.392), Ala417 (− 2.109), Tyr415 (− 2.162), Csy387 (− 2.145), Asn385 (− 1.345), Lys367 (− 2.113), Val365 (− 2.134), Leu363 (− 1.336), Gln336 (− 1.815), Asn324 (− 1.425), Gly321 (− 1.444), Phe320 (− 2.119), Asp318 (− 2.125), Leu317 (− 2.672), His132 (− 2.371), Csy129 (− 1.843), Val121 (− 1.473), Thr118 (− 3.192), Gly117 (− 4.264), Pro116 (− 3.359), Tyr60 (− 2.456), Ser59 (− 1.898), Arg58 (− 3.114), Trp16 (− 1.588)	Lys418 (− 8.155), Glu322 (− 2.303), Lys134 (− 1.621), Trp16 (− 1.492)	Arg58 (2.07)	His132 (2.76)/ Lys418 (2.47)

Table 2 continued

Entry	Docking score	Glide interaction energy (kcal/mol)	Per-residues interactions			
			Van der Waals (kcal/mol)	Coulombic (kcal/mol)	H-bonds (Å)	π–π/π–cation stacking (Å)
6g	− 8.366	− 55.768	Lys418 (− 3.418), Ala417 (− 2.161), Tyr415 (− 2.137), Csy387 (− 2.146), Asn385 (− 1.442), Lys367 (− 2.139), Val365 (− 2.203), Leu363 (− 1.434), Gln336 (− 1.835), Gly321 (− 1.534), Phe320 (− 2.239),318 (− 2.148), Leu317 (− 2.936), His132 (− 2.999), Csy129 (− 1.985), Val121 (− 1.565), Thr118 (− 3.222), Gly117 (− 4.315), Pro116 (− 3.443), Tyr60 (− 2.572), Ser59 (− 1.929), Arg58 (− 3.089), Trp16 (− 1.692)	Lys418 (− 8.271), Lys367 (− 1.495), Lys134 (− 1.645)	Arg58 (2.73), Tyr60 (1.79)	His132 (2.53)/ Lys418 (2.50)
6h	− 8.935	− 60.153	Lys418 (− 3.561), Ala417 (− 2.316), Tyr415 (− 2.863), Csy387 (− 2.859), Asn385 (− 1.481), Lys367 (− 2.459), Val365 (− 2.964), Leu363 (− 1.523), Gln336 (− 1.921), Gly321 (− 1.984), Phe320 (− 2.263), Asp318 (− 2.929), Leu317 (− 3.259), His132 (− 3.559), Csy129 (− 1.942), Val121 (− 1.888), Thr118 (− 3.513), Gly117 (− 4.667), Pro116 (− 4.141), Tyr60 (− 2.749), Ser59 (− 1.967), Arg58 (− 4.122), Trp16 (− 2.063)	Lys418 (− 11.452), Lys367 (− 2.039), Glu322 (− 2.908), Lys134 (− 1.974), Trp16 (− 1.495)	Arg58 (2.07)	His132 (2.771)/ Lys418 (2.479)

Table 2 continued

Entry	Docking score	Glide interaction energy (kcal/mol)	Per-residues interactions			
			Van der Waals (kcal/mol)	Coulombic (kcal/mol)	H-bonds (Å)	π–π/π–cation stacking (Å)
6i	− 6.285	− 38.62	Lys418 (− 1.318), Ala417 (− 1.133), Tyr415 (− 1.196), Asp389 (− 1.881), Csy387 (− 1.185), Asn385 (− 1.419), Phe369 (− 1.057), Phe366 (− 1.154), Val365 (− 1.31), Leu363 (− 1.198), Gln336 (− 1.973), 334 (− 1.078), Asn324 (− 1.517), Gly321 (− 1.479), Phe320 (− 1.176), Leu317 (− 1.662), His132 (− 1.025), Ile131 (− 1.114), Thr118 (− 1.011), Gly117 (− 1.165), Pro116 (− 1.681), Tyr60 (− 1.575), Arg58 (− 1.125),	Lys418 (− 4.672), Asp389 (− 1.73), Arg119 (− 0.931), Arg58 (− 1.359)	Gly117 (2.48)	His132 (3.053)
6j	− 6.147	− 35.872	Lys418 (− 1.189), Ala417 (− 1.13), Tyr415 (− 1.935), Csy387 (− 1.606), Asn385 (− 1.967), Lys367 (− 1.461), Val365 (− 1.297), Gln336 (− 1.498), Asp318 (− 1.932), Leu317 (− 1.026), His132 (− 1.274), Csy129 (− 1.28), Val121 (− 1.448), Thr118 (− 1.364), Gly117 (− 1.043), Pro116 (− 1.421), Tyr60 (− 1.616), Ser59 (− 1.412), Arg58 (− 1.626), Trp16 (− 1.141),	Lys418 (− 4.773)	Arg58 (2.27)	His132 (2.73)/ Lys418 (2.47)

Table 2 continued

Entry	Docking score	Glide interaction energy (kcal/mol)	Per-residues interactions			
			Van der Waals (kcal/mol)	Coulombic (kcal/mol)	H-bonds (Å)	π–π/π–cation stacking (Å)
6k	− 7.279	− 45.253	Lys418 (− 2.469), Ala417 (− 2.063), Tyr415 (− 2.046), Csy387 (− 1.959), Asn385 (− 1.111), Phe369 (− 1.201), Lys367 (− 1.553), Phe366 (− 1.139), Val365 (− 1.732), Leu363 (− 1.123), Gln336 (− 1.456), Gly321 (− 1.182), Phe320 (− 1.442), Leu317 (− 2.129), Tyr314 (− 1.063), Lys134 (− 2.006), Gly133 (− 1.414), Ile131 (− 1.1720, Csy129 (− 1.341), Gly125 (− 1.333), Val121 (− 1.102), Thr118 (− 1.895), Gly117 (− 2.645), Tyr60 (− 2.026), Ser59 (− 1.647), Arg58 (− 1.468), Trp16 (− 2.094)	Lys418 (− 5.777), Lys367 (− 2.488), Glu322 (− 2.122), Lys134 (− 2.586), Gly117 (− 1.03), Pro116 (− 1.52)	Lys418 (2.09)	His132 (2.37)

mycobacterial enzyme DprE1, providing ample opportunity to nurture this scaffold further through the structure-based drug design approach to arrive at high-affinity candidates.

In silico ADME predictions

We have performed a computational study for the prediction of ADME properties. The compounds exhibited a good % absorption (% ABS) ranging from 47.790 to 63.598% (Table 3) and calculated by % ABS = 109 − (0.345 × TPSA). We have calculated molecular weight (MW), molecular volume (MV), number of hydrogen bond donors (*n*-OHNH), number of hydrogen bond acceptors (*n*-ON), logarithm of partition coefficient (milog P), topological polar surface area (TPSA), number of rotatable bonds (*n*-ROTB) and Lipinski's rule of five [69] using the Molinspiration online property calculation toolkit [70]. The drug-likeness model score has been calculated by Molsoft software [71] (Table 3).

Table 3 Pharmacokinetic parameters important for good oral bioavailability

Entry	%ABS	*n*-atoms	TPSA (A^2)	*n*-ROTB	MV	MW	Milog *p*	*n*-ON	*n*-OHNH	Lipinski's violations	Drug-likeness model score
Rule	–	–	–	–	–	< 500	≤ 5	< 10	< 5	≤ 1	–
6a	63.598	36	131.60	4	397.27	479.45	3.95	9	2	0	0.64
6b	63.598	37	131.60	4	413.83	493.48	4.40	9	2	0	0.48
6c	60.413	38	140.83	5	422.82	509.47	4.17	10	2	1	0.20
6d	60.413	38	140.83	5	422.82	509.47	4.01	10	2	1	0.58
6e	63.598	37	131.60	4	410.81	513.89	4.79	9	2	1	0.44
6f	63.598	37	131.60	4	410.81	513.89	4.82	9	2	1	0.55
6g	63.598	37	131.60	4	410.81	513.89	4.63	9	2	1	0.77
6h	63.598	37	131.60	4	415.16	558.34	4.95	9	2	1	0.32
6i	47.790	39	177.42	5	420.61	524.45	4.07	12	2	2	0.29
6j	47.790	39	177.42	5	420.61	524.45	4.10	12	2	2	0.47
6k	47.790	39	177.42	5	420.61	524.45	3.91	12	2	2	0.46

Conclusions

We have demonstrated the synthesis of novel triazole-incorporated biscoumarin conjugates by using the molecular hybridization approach for the first time. The synthesized conjugates were evaluated for their in vitro antitubercular activity against dormant and active *Mtb* H37Ra strains. Most of the conjugates displayed good activity with IC_{50} values ranging from 1.44 to 20.00 μg/mL against both the *Mtb* H37Ra strains. In particular, compound **6h** exhibited excellent antitubercular activity with an IC_{50} value of 1.44 μg/mL against dormant *Mtb* H37Ra. A molecular docking study was performed against the mycobaterial target DprE1 to investigate the possible binding mode of the compounds. In addition, the conjugates showed excellent anti-oxidant activity with lower IC_{50} values than the standard drug BHT. These findings provide an opportunity to explore this scaffold as a pertinent starting point for structure-based lead optimization.

Acknowledgements One of the authors, A.B.D., is very grateful to the University Grants Commission, New Delhi, for the award of a research fellowship. The authors are also grateful to the Department of Chemistry, Dr. Babasaheb Ambedkar Marathwada University, Aurangabad-431 004, India, for providing necessary laboratory facilities. The authors are also grateful to Schrodinger, Inc. for providing the Demo license of the Schrodinger Molecular Modeling Suite to perform the molecular modeling studies.

References

1. X.Y. Huang, Z.J. Shan, H.L. Zhai, L. Su, X.Y. Zhang, Chem. Biol. Drug Des. **78**, 651 (2011)
2. M.A. Musa, J.S. Cooperwood, M.O.F. Khan, Curr. Med. Chem. **15**, 2664 (2008)
3. P.O. Patil, S.B. Bari, S.D. Firke, P.K. Deshmukh, S.T. Donda, D.A. Patil, Bioorg. Med. Chem. **21**, 2434 (2013)
4. I. Kostova, S. Bhatia, P. Grigorov, S. Balkansky, V.S. Parmar, A.K. Prasad, L. Saso, Curr. Med. Chem. **18**, 3929 (2011)
5. J.Y. Yeh, M.S. Coumar, J.T. Horng, H.Y. Shiao, F.M. Kuo, H.L. Lee, I.C. Chen, C.W. Chang, W.F. Tang, S.N. Tseng, C.J. Chen, S.R. Shih, J.T.A. Hsu, C.C. Liao, Y.S. Chao, H.P. Hsieh, J. Med. Chem. **53**, 1519 (2010)
6. K.V. Sashidhara, A. Kumar, M. Chatterjee, K.B. Rao, S. Singh, A.K. Verma, G. Palit, Bioorg. Med. Chem. Lett. **21**, 1937 (2011)
7. J. Neyts, E.D. Clercq, R. Singha, Y.H. Chang, A.R. Das, S.K. Chakraborty, S.C. Hong, S.C. Tsay, M.H. Hsu, J.R. Hwu, J. Med. Chem. **52**, 1486 (2009)
8. G. Melagraki, A. Afantitis, O.I. Markopoulou, A. Detsi, M. Koufaki, C. Kontogiorgis, D.J.H. Litina, Eur. J. Med. Chem. **44**, 3020 (2009)
9. S.H. Cardoso, M.B. Barreto, M.C.S. Lourenco, M.D.G. de Henriques, A.L.P. Candea, C.R. Kaiser, M.V.N. de Souza, Chem. Biol. Drug Des. **77**, 489 (2011)
10. K.M. Khan, F. Rahim, A. Wadood, N. Kosar, M. Taha, S. Lalani, A. Khan, M.I. Fakhri, M. Junaid, W. Rehman, M. Khan, S. Perveen, M. Sajid, M.I. Choudhary, Eur. J. Med. Chem. **81**, 245 (2014)
11. I. Manolov, C. Maichle-Moessmer, I. Nicolova, N. Danchev, Arch. Pharm. Chem. Life Sci. **339**, 319 (2006)
12. N. Hamdi, M.C. Puerta, P. Valerga, Eur. J. Med. Chem. **43**, 2541 (2008)
13. C.X. Su, J.F. Mouscadet, C.C. Chiang, H.J. Tsai, L.Y. Hsu, Chem. Pharm. Bull. **54**, 682 (2006)
14. M.A. Lodhi, Z. ul-Haq, A. Wadood, S. Iqbal, K.M. Khan, A. ur-Rahman, M.I. Choudhary, Med. Chem. Res. **22**, 498 (2013)
15. M. Faisal, A. Saeed, D. Shahzad, T.A. Fattah, B. Lal, P.A. Channar, J. Mahar, S. Saeed, P.A. Mahesar, F.A. Larik, Eur. J. Med. Chem. **141**, 386 (2017)

16. Y.P. Sui, H.R. Huo, J.J. Xin, J. Li, X.J. Li, X.L. Du, H. Ma, H.Y. Zhou, H.D. Zhan, Z.J. Wang, C. Li, F. Sui, M.K. Li, Molecules **20**, 17614 (2015)
17. V.D. Kancheva, P.V. Boranova, J.T. Nechev, I.I. Manolov, Biochimie **92**, 1138 (2010)
18. J. Xu, J. Ai, S. Liu, X. Peng, L. Yu, M. Geng, F. Nan, Org. Biomol. Chem. **12**, 3721 (2014)
19. F.G. Medina, J.G. Marrero, M.M. Alonso, M.C. Gonzalez, I.C. Guerrero, A.G.T. Garcia, S.O. Robles, Nat. Prod. Rep. **32**, 1472 (2015)
20. H.C. Kolb, M.G. Finn, K.B. Sharpless, Angew. Chem. Int. Ed. **40**, 2004 (2001)
21. F. Amblard, J.H. Cho, R.F. Schinazi, Chem. Rev. **109**, 4207 (2009)
22. S.G. Agalave, S.R. Maujan, V.S. Pore, Chem. Asian J. **6**, 2696 (2011)
23. V.K. Tiwari, B.B. Mishra, K.B. Mishra, N. Mishra, A.S. Singh, X. Chen, Chem. Rev. **116**, 3086 (2016)
24. K. Kacprzak, I. Skiera, M. Piasecka, Z. Paryzek, Chem. Rev. **116**, 5689 (2016)
25. J.M. Holub, K. Kirshenbaum, Chem. Soc. Rev. **39**, 1325 (2010)
26. I.E. Valverde, A. Bauman, C.A. Kluba, S. Vomstein, M.A. Walter, T.L. Mindt, Angew. Chem. Int. Ed. **52**, 8957 (2013)
27. I. Mohammed, I.R. Kummetha, G. Singh, N. Sharova, G. Lichinchi, J. Dang, M. Stevenson, T.M. Rana, J. Med. Chem. **59**, 7677 (2016)
28. E. Bonandi, M.S. Christodoulou, G. Fumagalli, D. Perdicchia, G. Rastelli, D. Passarella, Drug Discovery Today **22**, 1572 (2017)
29. D. Gonzaga, M.R. Senger, F.C. Silva, V.F. Ferreira, F.P. Silva-Jr, Eur. J. Med. Chem. **74**, 461 (2014)
30. X.L. Wang, K. Wan, C.H. Zhou, Eur. J. Med. Chem. **45**, 4631 (2010)
31. Z.C. Dai, Y.F. Chen, M. Zhang, S.K. Li, T.T. Yang, L. Shen, J.X. Wang, S.S. Qian, H.L. Zhu, Y.H. Ye, Org. Biomol. Chem. **13**, 477 (2015)
32. L. Zhou, A. Amer, M. Korn, R. Burda, J. Balzarini, E. De Clercq, E.R. Kern, P.F. Torrence, Antiviral Chem. Chemother. **16**, 375 (2005)
33. K. Dabak, O. Sezer, A. Akar, O. Anac, Eur. J. Med. Chem. **38**, 215 (2003)
34. M.S. Costa, N. Boechat, E.A. Rangel, F.C. Silva, A.M.T. de Souza, C.R. Rodrigues, H.C. Castro, I.N. Junior, M.C.S. Lourenco, S.M.S.V. Wardell, V.F. Ferreira, Bioorg. Med. Chem. **14**, 8644 (2006)
35. B.K. Singh, A.K. Yadav, B. Kumar, A. Gaikwad, S.K. Sinha, V. Chaturvedi, R.P. Tripathi, Carbohydr. Res. **343**, 1153 (2008)
36. R.P. Tripathi, A.K. Yadav, A. Ajay, S.S. Bisht, V. Chaturvedi, S.K. Sinha, Eur. J. Med. Chem. **45**, 142 (2010)
37. K.D. Thomas, A.V. Adhikari, I.H. Chowdhury, E. Sumesh, N.K. Pal, Eur. J. Med. Chem. **46**, 2503 (2011)
38. N. Boechat, V.F. Ferreira, S.B. Ferreira, M.L.G. Ferreira, F.C. Silva, M.M. Bastos, M.S. Costa, M.C.S. Lourenco, A.C. Pinto, A.U. Krettli, A.C. Aguiar, B.M. Teixeira, N.V. Silva, P.R.C. Martins, F.A.F.M. Bezerra, A.L.S. Camilo, G.P. Silva, C.C.P. Costa, J. Med. Chem. **54**, 5988 (2011)
39. M.H. Shaikh, D.D. Subhedar, F.A.K. Khan, J.N. Sangshetti, B.B. Shingate, Chin. Chem. Lett. **27**, 295 (2016)
40. W. Zhang, Z. Li, M. Zhou, F. Wu, X. Hou, H. Luo, H. Liu, X. Han, G. Yan, Z. Ding, R. Li, Bioorg. Med. Chem. Lett. **24**, 799 (2014)
41. K. Kushwaha, N. Kaushik, S.C.Jain Lata, Bioorg. Med. Chem. Lett. **24**, 1795 (2014)
42. P.L. Rojas, M. Janeczko, K. Kubinski, A. Amesty, M. Masłyk, A.E. Braun, Molecules **23**, 199 (2018)
43. R.A. Kusanur, M.V. Kulkarni, Indian J. Chem. **44B**, 591 (2005)
44. S.G. Ouellet, D. Gauvreau, M. Cameron, S. Dolman, L.C. Campeau, G. Hughes, P.D.O. Shea, I.W. Davies, Org. Process Res. Dev. **16**, 214 (2012)
45. H.A. Stefani, K. Gueogjan, F. Manarin, S.H.P. Farsky, J.Z. Schpector, I. Caracelli, S.R.P. Rodrigues, M.N. Muscara, S.A. Teixeira, J.R. Santin, I.D. Machado, S.M. Bolonheis, R. Curi, M.A. Vinolo, Eur. J. Med. Chem. **58**, 117 (2012)
46. R. Pingaew, A. Saekee, P. Mandi, C. Nantasenamat, S. Prachayasittikul, S. Ruchirawat, V. Prachayasittikul, Eur. J. Med. Chem. **85**, 65 (2014)
47. R.J. Naik, M.V. Kulkarni, K.S.R. Pai, P.G. Nayak, Chem. Biol. Drug Des. **80**, 516 (2012)
48. M.H. Shaikh, D.D. Subhedar, B.B. Shingate, F.A.K. Khan, J.N. Sangshetti, V.M. Khedkar, L. Nawale, D. Sarkar, G.R. Navale, S.S. Shinde, Med. Chem. Res. **25**, 790 (2016)
49. A. Anand, M.V. Kulkarni, S.D. Joshi, S.R. Dixit, Bioorg. Med. Chem. Lett. **26**, 4709 (2016)
50. A. Anand, R.J. Naik, H.M. Revankar, M.V. Kulkarni, S.R. Dixit, S.D. Joshi, Eur. J. Med. Chem. **105**, 194 (2015)
51. H.R. Dholariya, K.S. Patel, J.C. Patel, K.D. Patel, Spectrochim. Acta A **108**, 319 (2013)

52. D. Ashok, S. Gundu, V.K. Aamate, M.G. Devulapally, R. Bathini, V. Manga, J. Mol. Struct. **1157**, 312 (2018)
53. N.S. Chandrasekera, T. Alling, M.A. Bailey, M. Files, J.V. Early, J. Ollinger, Y. Ovechkina, T. Masquelin, P.V. Desai, J.W. Cramer, P.A. Hipskind, J.O. Odingo, T. Parish, J. Med. Chem. **58**, 7273 (2015)
54. R.P. Tripathi, N. Tewari, N. Dwivedi, V.K. Tiwari, Med. Res. Rev. **25**, 93 (2005)
55. L. Pulipati, J.P. Sridevi, P. Yogeeswari, D. Sriram, S. Kantevari, Bioorg. Med. Chem. Lett. **26**, 3135 (2016)
56. D.D. Vita, F. Pandolfi, R. Cirilli, L. Scipione, R.D. Santo, L. Friggeri, M. Mori, D. Fiorucci, G. Maccari, R.S.A. Christopher, C. Zamperini, V. Pau, A.D. Logu, S. Tortorella, M. Botta, Eur. J. Med. Chem. **121**, 169 (2016)
57. W.A. Yehye, N.A. Rahman, A. Ariffin, S.B.A. Hamid, A.A. Alhadi, F.A. Kadir, M. Yaeghoobi, Eur. J. Med. Chem. **101**, 295 (2015)
58. J.C.J.M.D.S. Menezes, S.P. Kamat, J.A.S. Cavaleiro, A. Gaspar, J. Garrido, F. Borges, Eur. J. Med. Chem. **46**, 773 (2011)
59. M.H. Shaikh, D.D. Subhedar, L. Nawale, D. Sarkar, F.A.K. Khan, J.N. Sangshetti, B.B. Shingate, Med. Chem. Commun. **6**, 1104 (2015)
60. D.D. Subhedar, M.H. Shaikh, B.B. Shingate, L. Nawale, D. Sarkar, V.M. Khedkar, Med. Chem. Commun. **7**, 1832 (2016)
61. D.D. Subhedar, M.H. Shaikh, L. Nawale, A. Yeware, D. Sarkar, F.A.K. Khan, J.N. Sangshetti, B.B. Shingate, Bioorg. Med. Chem. Lett. **26**, 2278 (2016)
62. D.D. Subhedar, M.H. Shaikh, F.A.K. Khan, J.N. Sangshetti, V.M. Khedkar, B.B. Shingate, New J. Chem. **40**, 3047 (2016)
63. M.H. Shaikh, D.D. Subhedar, M. Arkile, V.M. Khedkar, N. Jadhav, D. Sarkar, B.B. Shingate, Bioorg. Med. Chem. Lett. **26**, 561 (2016)
64. D.D. Subhedar, M.H. Shaikh, M.A. Arkile, A. Yeware, D. Sarkar, B.B. Shingate, Bioorg. Med. Chem. Lett. **26**, 1704 (2016)
65. M.H. Shaikh, D.D. Subhedar, F.A.K. Khan, J.N. Sangshetti, L. Nawale, M. Arkile, D. Sarkar, B.B. Shingate, J. Heterocycl. Chem. **54**, 413 (2017)
66. D.D. Subhedar, M.H. Shaikh, B.B. Shingate, L. Nawale, D. Sarkar, V.M. Khedkar, F.A.K. Khan, J.N. Sangshetti, Eur. J. Med. Chem. **125**, 385 (2017)
67. R.A. Friesner, R.B. Murphy, M.P. Repasky, L.L. Frye, J.R. Greenwood, T.A. Halgren, P.C. Sanschagrin, D.T. Mainz, J. Med. Chem. **49**, 6177 (2006)
68. U. Singh, S. Akhtar, A. Mishra, D. Sarkar, J. Microbiol. Methods **84**, 202 (2011)
69. C.A. Lipinski, F. Lombardo, B.W. Dominy, P.J. Feeney, Adv. Drug Delivery Rev. **46**, 3 (2001)
70. http://www.molinspiration.com/cgibin/properties
71. http://www.molsoft.com/mprop/